Final Report

Project Title:	"Development and Demonstration of an Innovative Thermal Energy Storage System for Baseload Power Generation"
Project Period:	01/01/2011 – 07/31/2012
Current Phase Period:	01/01/2011 – 07/31/2012
Reporting Period:	01/01/2011 – 07/31/2012
Reporting Frequency:	Quarterly
Submission Date:	08/30/2012
Recipient:	University of South Florida
Recipient DUNS#:	069687242
Address:	4202E. Fowler Avenue ENB 118 Tampa FL. 33620
Website:	www.cerc.eng.usf.edu
Award Number:	DE-EE0003590
Awarding Agency:	DOE EERE SETP CSP subprogram
Working Partners:	Sunborne Energy Technologies, Inc.
Cost-Sharing Partners:	Sunborne Energy Technologies, Inc. USF Florida Energy Systems Consortium
Principal Investigator:	Dr. Yogi Goswami John and Naida Ramil Professor and Co-Director CERC Phone: 813-974-0956 Fax: 813-974-2050 Email: goswami@usf.edu
GO Contracting Officer:	Golden, CO
Technology Project Officer:	GO/HQ TPO
DOE Technical Manager:	HQ Technical Lead

Project Objective:

The objective of this project is to research and develop a thermal energy storage system (operating range 300^0C – 450 ^{0}C) based on encapsulated phase change materials (PCM) that can meet the utility-scale base-load concentrated solar power plant requirements at much lower system costs compared to the existing thermal energy storage (TES) concepts. The major focus of this program is to develop suitable encapsulation methods for existing low-cost phase change materials that would provide a cost effective and reliable solution for thermal energy storage to be integrated in solar thermal power plants. This project proposes a TES system concept that will allow for an increase of the capacity factor of the present CSP technologies to 75% or greater and reduce the cost to less than \$20/kWh$_t$.

Introduction:

In this project, we plan to prepare porous pellets of phase change materials and coat them with the encapsulation material using low cost coating techniques. The porous pellets will allow for the volumetric expansion during PCM melting and hence impose less stress on the shell material. There are two major challenges to the success of this concept:

1. Forming porous macro-spheres of the PCM material at optimum size and the optimum pore volume in the macro-spheres that will account for the volume change from solid to liquid phase.
2. Encapsulating the macro-spheres of PCM in a higher melting temperature material at low cost.

Project Approach:

Porous pellets are prepared to achieve the required void space, shape and size. Encapsulation is achieved by coating using an industrial process. Characterization of the PCM and pellets is done using a Differential Scanning Calorimeter (DSC), SDT-600 (which is simultaneously a Differential Scanning Calorimeter (DSC) and a Thermogravimetric analyzer (TGA)), FTIR, XFA 500 (for thermal diffusivity) and a Leinz optical microscope (for coating thickness).

Project Results and Discussion:

Task 1.0 Preparation of PCM pellets and coating

Subtask 1.1 Fabrication of Porous PCM Pellets

For fabrication of porous pellets methods such as prilling, granulation and hydraulic pressing were investigated. It was found that a typical size of prills fabricated using the prilling process varies from 1mm to 3 mm. The granulation technique requires the use of binders for forming the granules, which could have adverse effect on the properties of the PCM and/or the subsequent behavior of the pellets . The hydraulic pressing method was determined to be the best option for our application.

We observed that by the pressing technique, pellets with a maximum porosity of 5% could be made. Improvement of this process to achieve a void-space/porosity of 15% or more was investigated. The method that can provide the required volumetric expansion space by providing

a void in the PCM pellet is shown in Fig.1 below. Therefore, pellets with the required void space were prepared by this method.

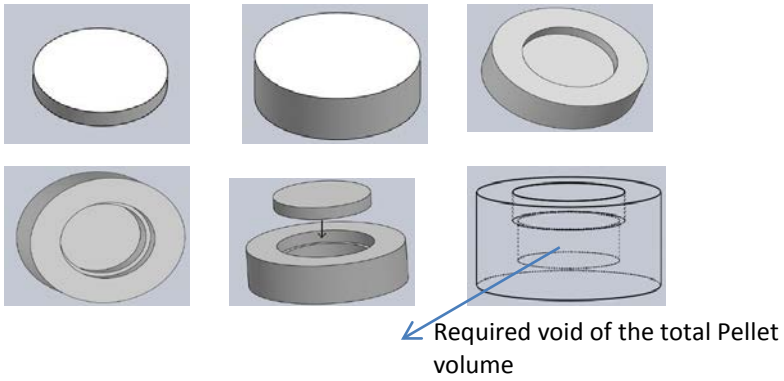

Fig. 1: Provision for volumetric expansion space

We also developed a technique to prepare spherical pellets with a void in the center. These pellets were made with a die and a hydraulic press (Figures 2a and 2b). Upon heating the coated pellet, the air pressure in the void rises. A pinhole was drilled in the pellet to help some air escape after heating, as shown in Fig. 2b. The drilled and undrilled hemispheres were then joined together with a polyimide and silicon carbide mixture. The joint was cured in a furnace and allowed to sit in the furnace at high temperature. During this time the pinhole was open. The air inside the void escaped through the pinhole at this higher temperature, after which, the pinhole was closed with the polyimide and silicon carbide mixture. This created a vacuum in the sphere upon cooling.

Figure 2a. Hemispherical Pellets.

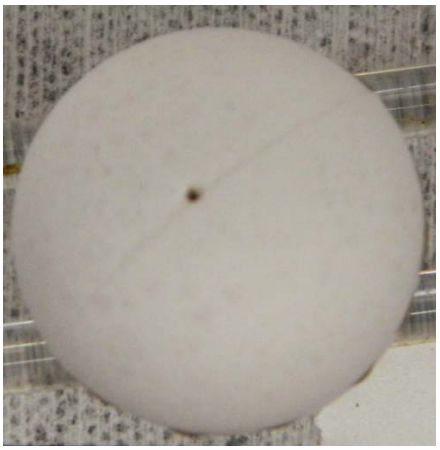

Figure 2b. Spherical Pellet with a Pinhole

Subtask 1.2 Encapsulation of PCM pellets

We started our experiments for encapsulation by dip coating of sodium nitrate pellets in molten zinc, however, it was noticed molten zinc did not wet the salt pellets. It was, therefore, concluded that a surface treatment is necessary before dipping the pellets in a molten metal. Surface treatment using a sodium silicate solution aided in coating molten zinc on the pellet, but resulted in a non-uniform coating with air-bubble formation. Powdered zinc was used to encapsulate the pellets using the powder metallurgy technique, but the coating cracked when the pellet was heated.

In another approach, a PCM (sodium nitrate) pellet was encapsulated by depositing a primary layer of polyimide (PI) that was followed by a chemical method for depositing a silicon dioxide (SiO_2) layer on top of the polyimide layer. The encapsulated pellets were tested for high temperature stability by heating them above the melting point of the PCM. The capsules were tested for cyclic stability by heating from room temperature to 350^0C at a heating rate of 4^0C/min, a dwell time of 2 hours at 350^0C and then cooled to 280^oC. In another test, a mixture of PI and SiC (silicon carbide) was prepared and coated on the PCM pellet followed by silicon dioxide coating.

The industrial process for PI coating on a PCM pellets:

In order to develop an automated industrial encapsulation process, a Laboratory Development model of an industrial Coating System (LDCS) was used for coating on the PCM pellets. Figure 5 shows the LDCS coater. Figure 6 shows how liquid is used to flow in the LDCS coater. Spray coating in the machine helps to maintain a uniform coat around the spherical pellets. Figure 7 shows the pellets that were used in this machine for coating. Figure 8 shows a cured PCM with a layer of coating. Figure 9 shows multi-layered coated PCM pellets.

Figure 5. LDCS coater

Figure 6: LDCS coater: Pump

Figure 7. The pellets used in the coater

Figure 8. One layer coated PCM pellets

Figure 9. Multi-layered coating process

Finally, another method was developed for coating the pellets, which has worked successfully. Figure 10 shows a capsule prepared by this method.

Figure 10: A PCM Capsule

Task 2.0 Characterization of PCM pellets

DSC (differential scanning calorimetry) measurements were carried out on some of the salts listed in Table 1 to characterize the latent heat and melting point of the PCM. It was found that there is a large difference between the measured and published values of latent heats of the materials, which can be due to:

- Purity of the sample
- Presence of moisture in the case of hygroscopic materials

A eutectic of Li_2CO_3 and Na_2CO_3 salts was prepared and characterized. The published /theoretical value for latent heat of this eutectic is 370 kJ/kg and the published melting point is 495.8˚C (Janz et al., 1979). Two different methods were used for the preparation of the eutectics:

- Weighing the individual salts in the required ratio and mixing them in the ball mill
- Mixing using a mortar and pestle

Table 1: Phase change materials being considered for the study

PCM	Melting temperature (^{0}C)		Latent heat of fusion (kJ/kg)	
	Published	Measured	Published	Measured
$NaNO_3$	307	303	172-177	170
KNO_3	333	334	88 – 266	108
26.8% NaCl – 73.2% NaOH	370	354	370	138
56 wt% NaCl – 44% $MgCl_2$	430	434	320	168
33 wt% NaCl – 67 % $CaCl_2$	500	502	239 – 282	193

For comparison, samples were also prepared in different environments, i.e., complete exposure to air during mixing and minimum exposure to air (only during transferring the sample to DSC). Table 2 shows the results obtained.

Table 2: DSC Results for Li_2CO_3/Na_2CO_3 eutectic

Method	Melting temperature (^{0}C)	Latent heat of fusion (kJ/kg)
Samples exposed air (graphite pans)	497.49	199.8
Mortar and Pestle (ceramic pans)	505.85	255.4
Ball Milling in air (ceramic pans)	502.87	243.4
Ball Milling in nitrogen (ceramic pans)	501.52	253.6

The following conclusions are drawn from the study.

- The samples should not be exposed to air
- The latent heat of the eutectic is 250 – 255 kJ/kg as compared to the published value of 370 kJ/kg.
- Both the preparation methods result in almost the same value of latent heat

A eutectic of $MgCl_2$-KCl-NaCl having a composition of 60wt% $MgCl_2$-20.4%KCl-19.6%NaCl was investigated as a potential PCM candidate. Its melting point and latent heat of fusion were measured by a Differential Scanning Calorimeter (DSC), SDT-600 (which is a simultaneous DSC and Thermogravimetric analyzer (TGA)) and compared with similar data from NREL. The results are reported in Table 3. The purity of single salt components was as follows; $MgCl_2$ = 99.99%, KCl = 99.997%, and NaCl= 99.999%. The melting point of this eutectic is given in the literature (Solar Energy, 2007, 81: 829–837) as 380^{o}C and theoretical latent heat is given as 400kJ/Kg. As can be seen from Table 3, the measured latent heat of fusion values are about half of the theoretical value reported in the literature. However, our values are slightly higher than those of NREL perhaps due to the purity of the chemicals. The results from two independent sources show that the actual latent heat value is less than the theoretical value reported.

Table 3. Latent Heat of fusion $MgCl_2$-KCl-NaCl eutectic (60wt% $MgCl_2$-20.4%KCl-19.6%NaCl)

	Average Latent Heat (kJ/kg)	First Cycle Latent Heat (kJ/kg)	Second Cycle Latent Heat (kJ/kg)	Third Cycle Latent Heat (kJ/kg)
USF DSC	230.73	222.1	235.8	234.3
USF SDT-600	232.56	221.1	238.4	238.2
NREL data	198.34	197.92	199.50	197.59

Task 3.0 Testing of PCM pellets

Thermal cycling was performed on the capsule using the following procedure. The pellet is kept in the furnace, near the thermocouple, and is heated up to 325^{o}C, which is above the melting temperature of the PCM in the capsule. It is then dwelled at 325^{o}C for 1 hour, after which it is cooled to 250^{o}C. Since the sodium nitrate melts at 306^{o}C, cooling to 250^{o}C ensures that the salt solidifies prior to subsequent cycling. Passing a thermal cycle means that the salt is melted completely within the capsule, followed by complete solidification without any leakage of salt from the capsule. Figure 11 shows a capsule, which has successfully gone over 200 thermal cycles, which is higher than the Phase I goal of 50 cycles. Discoloration of the metal coat is due to oxidation of the outer metal layer, turning into a metal oxide. This is a natural occurrence since the pellet is being heated in air, which is an oxidizing environment.

Figure 11: After 200 Thermal Cycles

Task 4.0 Numerical analysis of the PCM pellet

In this task, numerical models have been developed to simulate fluid dynamics, heat transfer, and phase change that occur during the melting of sodium nitrate ($NaNO_3$) encapsulated in a metallic spherical shell and subjected to a constant temperature boundary condition above its melting point at the outer wall of the shell. In this task, two different problems have been investigated, namely, completely filled capsule and capsule with void space. Both of these problems have been modeled by solving equations for the conservation of mass, momentum, and energy numerically using a control volume discretization approach along with the enthalpy-porosity method to track the melting front.

In the completely filled model, a spherical shell of thickness t, under the gravitational field, is entirely filled with a solid phase change material (PCM) at temperature T_i, where T_i is slightly below the PCM melting temperature T_m. For time $t>0$, a constant temperature boundary condition T_w is applied on the outer surface of the shell, which is greater than the melting temperature of the PCM.

In the void space model, the previously considered spherical shell is partially filled with solid $NaNO_3$ and the remaining volume is occupied by air. The air space provides room for volumetric expansion during the phase change process. In this model, a volume-tracking algorithm is used to track the motion of the PCM/Air interface. The ideal gas equation of state is used for air and the same constant temperature boundary condition is imposed at the outer surface of the shell.

Numerically predicted results from both models are presented in this report. It may be noted that fluid flow and heat transfer in the capsule is axisymmetric around the vertical axis of the sphere and conduction is the only mode of heat transfer through the solid shell material. The models used the following assumptions: (1) both solid and liquid phases are homogeneous and isotropic, (2) the liquid phase is a viscous Newtonian fluid, (3) the flow is laminar and has no viscous dissipation, (4) the Boussinesq approximation can be used to model natural convection in the liquid phase, (5) the thermal conductivity and specific heat in the PCM varies with temperature, (6) the whole system is initially sub-cooled at 303.8 ºC, and (7) melting of $NaNO_3$ takes place in the interval of 306.3-306.8ºC where the density in the mushy zone varies linearly from 2118 kg/m^3 at 306.3 ºC to 1904 kg/m^3 at 306.8ºC. The material properties and input parameters are listed in Table 4.

The predicted temperature field, PCM solid phase distribution, and liquid phase stream line contours, during the melting of a 40mm internal diameter capsule without void space, as a function of dimensionless time defined by the product of Ste and Fo are presented in composite diagrams in Fig. 12. The temperature distribution of the system is presented on the left hand side of each circle while the right hand side contains the PCM solid phase presented in black and the stream line contours.

Table 4. Material properties and input parameters.

Shell material (Aluminum)	
$\rho = 2719\ kg\ m^{-3}$	
$c_p = 871\ J\ kg^{-1}K^{-1}$	
$k = 202.4\ W\ m^{-1}K^{-1}$	
PCM material ($NaNO_3$)	
$T > 306.8°C$	$\rho = \rho_l/\beta(T - T_l) + 1$
$304.8°C < T \leq 306.8°C$	$\rho = 63958.65 - 107T\ kg\ m^{-3}$
$303.8°C \leq T \leq 304.8°C$	$\rho_s = 2118\ kg\ m^{-3}$
$T > 304.8°C$	$k_l = 0.565 + 44.73x10^{-5}(T - 579.9)\ W\ m^{-1}\ K^{-1}$
$303.8°C \leq T \leq 304.8°C$	$k_s = 0.565 + 33.49x10^{-5}(T - 230.0)\ W\ m^{-1}\ K^{-1}$
$T > 303.8°C$	$c_{ps} = c_{pl} = 444.53 + 2.18T\ J\ kg^{-1}\ K^{-1}$
$T > 306.8°C$	$\mu = 3.02x10^{-3}\ kg\ m^{-1}\ s^{-1}$
Input Parameters	
$T_m = 306.8°C$	
$T_i = 303.8°C$	
$\rho_l = 1904\ kg\ m^{-3}$	
$\beta = 6.6x10^{-4}K^{-1}$	
$L = 182000\ J\ kg^{-1}$	

At the beginning of the process (Fig. 12a), heat is transferred by conduction through the capsule wall into the PCM due to the temperature difference between the wall and the initial temperature of the system. The temperature distribution in the PCM is similar to the solution of the Laplace equation, i.e. the isotherms have a concentric ring shape, independent of the polar angle. This suggests that the dominant transport phenomenon is heat conduction. Melting is initiated and an axisymmetric thin layer of molten PCM is created adjacent to the inner wall of the capsule as seen on the right hand side of Fig. 12a. As the melted portion grows larger (Figs. 12b, 12c, 12d) with time, a buoyancy induced motion is introduced in the liquid phase due to the lower density of the liquid in the vicinity of the inner surface of the aluminum shell. As the heated fluid moves up and covers the top region of the solid fraction, the rate of heat transfer from the wall to the solid PCM increases. The buoyancy induced recirculating flow enhances the melting process in this zone and the solid adopts an oblate spheroid-shape on the top. As the melting process proceeds, the solid portion shrinks in size and the recirculating flow grows in physical extent (Figs. 12e - 12i).

For the no void case, the numerically predicted liquid mass fraction as a function of time for different capsule diameters at the same Stefan number is presented in Fig. 13a. Faster melting takes place in a capsule with a smaller diameter with the total melting time of 11.2, 19.7, 24.8 and 34.1 minutes for pellets with 20, 30, 40 and 50mm internal diameter, respectively. In order to investigate the role of natural convection heat transfer that is characterized by the Grashof number, the liquid mass fraction for different capsule sizes is plotted in Fig. 13b as a function of dimensionless time that is defined as the product of the Stefan and Fourier numbers. It can be observed that a faster melting occurs with an increase in the Grashof number when the Stefan number is kept at a constant value of 0.047.

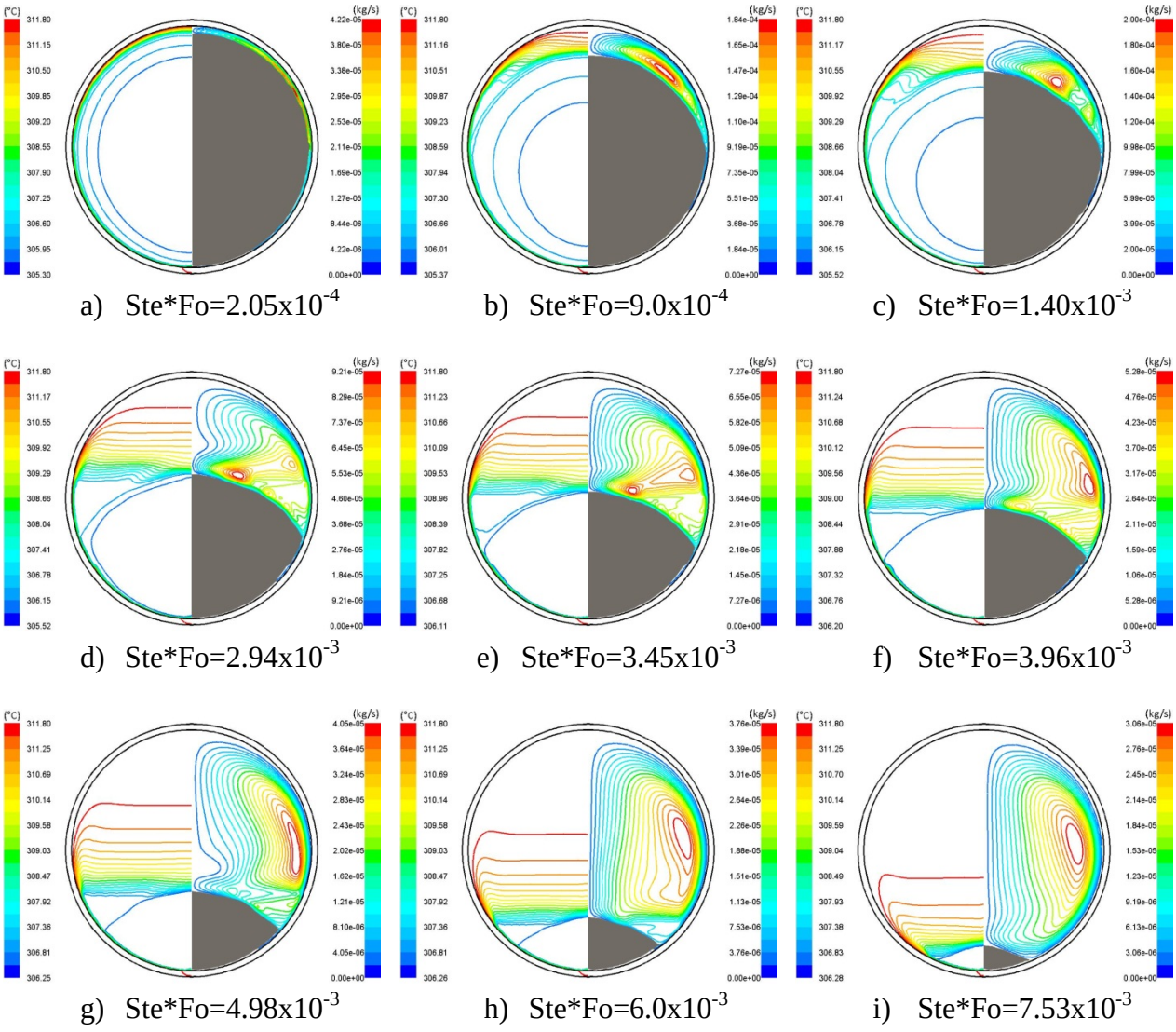

a) Ste*Fo=2.05x10^{-4} b) Ste*Fo=9.0x10^{-4} c) Ste*Fo=1.40x10^{-3}

d) Ste*Fo=2.94x10^{-3} e) Ste*Fo=3.45x10^{-3} f) Ste*Fo=3.96x10^{-3}

g) Ste*Fo=4.98x10^{-3} h) Ste*Fo=6.0x10^{-3} i) Ste*Fo=7.53x10^{-3}

Figure 12. PCM melting as a function of dimensionless time for a 40mm ID capsule, T_w-T_m =5°C.

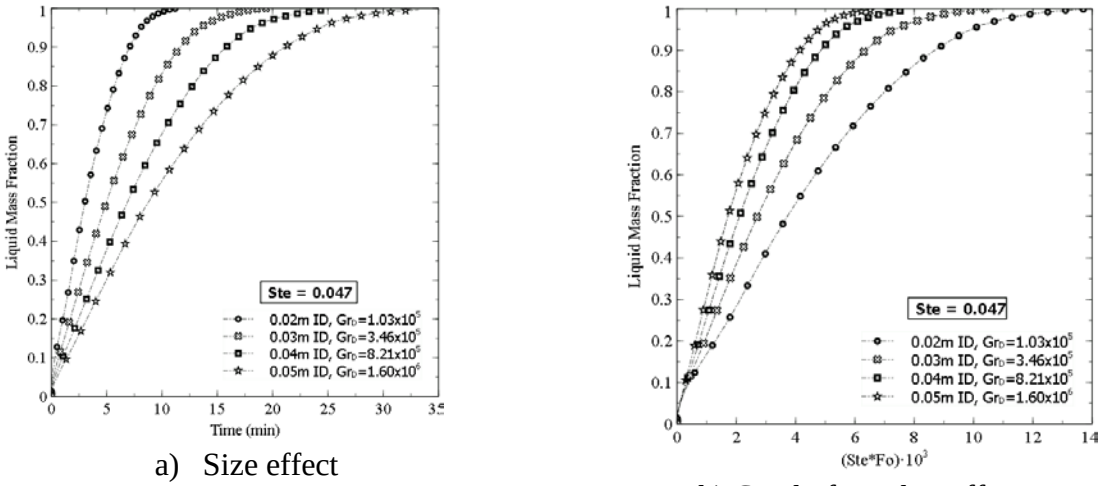

a) Size effect

b) Grashof number effect

Figure 13. Computed liquid mass fraction for different capsule sizes.

The above mentioned features are also seen when a void space is provided in the capsule. The results for the model with the void space filled with air are presented in Figs. 14-16. Table 5 shows the parameters used for different cases studied in this category. Due to volumetric expansion of the liquid phase, the PCM progressively fills up the pellet, as shown on the right hand side of Fig. 14. Consequently the air is compressed, increasing the pressure inside the pellet. In order to easily track the motion of the Air/PCM interface as a result of the thermal expansion, a red horizontal line is included on the right side of all the presented plots in Fig. 14, indicating the initial location of the interface. Also the interface height from the bottom is indicated in each plot in Fig. 14. Analogous to the results presented in Fig. 12, natural convection recirculation provides melting of the top of the solid PCM and the solid volume shrinks with time. Even though not illustrated in these plots, after the complete melting of the solid PCM has taken place, the natural convection heat transfer continues to mix the hot fluid adjacent to the wall with cold fluid away from the wall eventually bringing the system to an equilibrium isothermal condition.

Table 5. Computational cases studied with void space.

Case	*D_i (m)*	*$T_w - T_m$*	*Gr_D*	*Ste*
1	0.02	5	1.03×10^5	0.047
2	0.03		3.46×10^5	
3	0.04		8.21×0^5	
4	0.05		1.60×10^6	
5	0.0317	10	8.20×10^5	0.094
6	0.0291	13.5	8.49×10^5	0.128

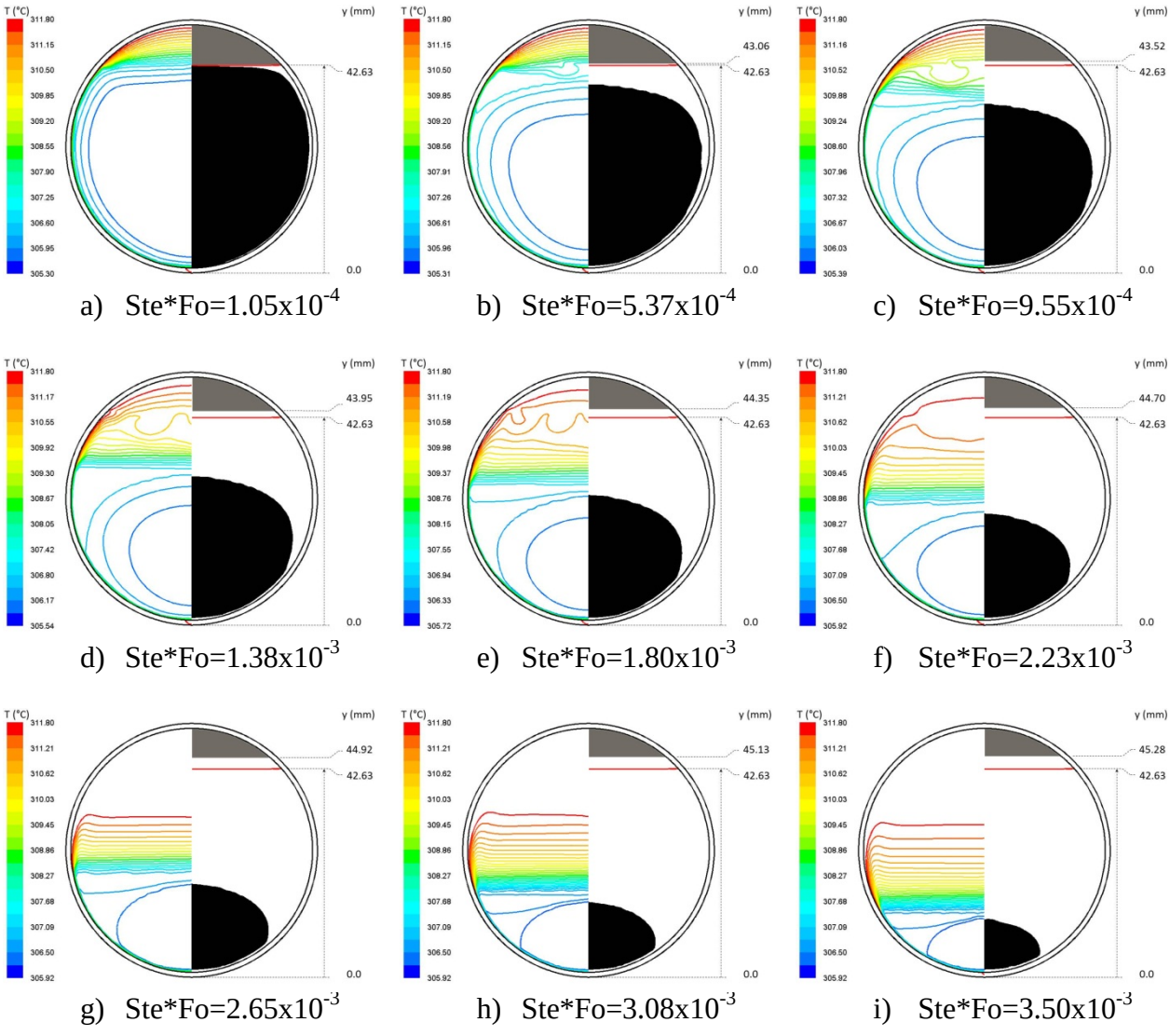

a) Ste*Fo=1.05x10^{-4} b) Ste*Fo=5.37x10^{-4} c) Ste*Fo=9.55x10^{-4}

d) Ste*Fo=1.38x10^{-3} e) Ste*Fo=1.80x10^{-3} f) Ste*Fo=2.23x10^{-3}

g) Ste*Fo=2.65x10^{-3} h) Ste*Fo=3.08x10^{-3} i) Ste*Fo=3.50x10^{-3}

Figure 14. PCM melting as a function of dimensionless time for a 50mm ID capsule, Tw-Tm =5°C

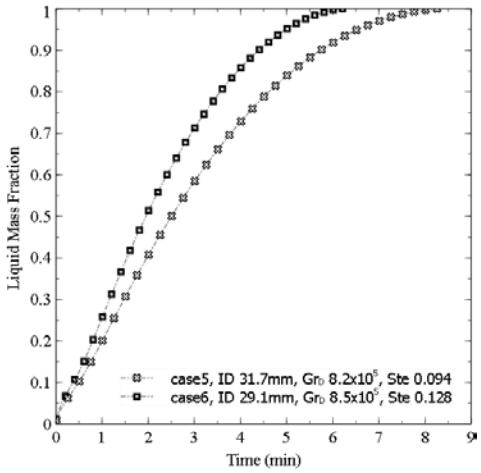

Figure 15. Stefan number effect

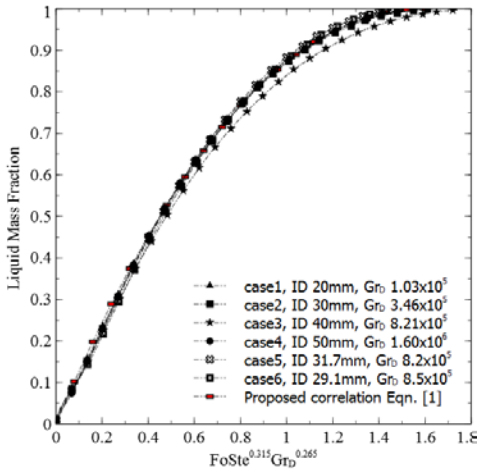

Figure 16. Generalized results

In order to investigate the effect of the Stefan number on the melting process for a given Grashof number, two study cases (5 and 6) have been compared in Fig. 15. The Grashof numbers for these two cases were made very close to each other by manipulating the temperature difference and the pellet size while they have different Stefan numbers. The numerically computed liquid mass fraction for these cases is plotted in Fig. 16. It can be inferred that a faster rate of melting is achieved when the Stefan number is higher, with total melting time of 8.30 and 6.24 minutes for the cases with T_w-T_m, equal to 10 and 13.5°C, respectively. The increase in the wall temperature enhances the sensible heat storable in the pellet and decreases the melting time.

Melt fractions for all the analyzed cases under the void space model are plotted as a function of combinations of Fourier, Stefan and Grashof numbers in Fig. 16 in order to develop a generalized correlation. By manipulating the exponents of the Stefan and Grashof numbers, it was determined that all the melt fraction curves converge to a single location when the exponent of the Stefan number is 0.315 and the exponent of the Grashof number is 0.265. It may be noted that the Grashof number is added to the previous dimensionless time formulation to include the influence of buoyancy on PCM melting in spherical enclosures. An equation for the generalized melt fraction curve can be written as:

$$MF = 1 - \left[1 - \frac{Fo\,Ste^{0.315}\,Gr^{0.265}}{1.6}\right]^{2.1} \qquad (1)$$

This correlation is valid in a range encompassing the cases simulated: $0.047 < Ste < 0.128$, $1.03 \times 10^5 < Gr_D < 1.6 \times 10^6$ and for Sodium Nitrate as the PCM material.

Task 5.0 Cost Analysis

Manufacturing plan sketch and preliminary cost analysis:

Following are the series of important steps envisioned in a continuous manufacturing of PCM pellets. A schematic of the manufacturing process is illustrated in the flowchart as shown below.

1. Preparation of PCM material (Feeder, Vibrator, Mixer etc.)
2. Production of PCM pellets (Rotary press)
3. Surface preparation of PCM using a thermal treatment
4. Precursor Coating of PCM pellets
5. Post processing of PCM pellets after coating with thermal treatment
6. Metal coating

The preliminary cost analysis is calculated considering the cost of a representative PCM material, equipment cost and other processing operational costs involved in the manufacturing of PCM pellets at an industrial level. The cost analysis is provided on the basis of the amount of PCM material that would be required to produce $1kWh_{th}$ energy.

$$\mathbf{Q = mCp_s\Delta T_1 + m\lambda + mCp_l\Delta T_2}$$

For Q = $1kWh_{th}$ energy (3.6×10^6 J); and considering the temperature range for $NaNO_3$ as 250° - 340° C (523 – 613 K), with melting point as 307° C (580 K);
Cps = 1.69 J/g K;
Cpl = 1.8 J/g K;
λ = 170 J/g;
$\Delta T_1 = 580 - 523 = 57$ K
$\Delta T_2 = 613 - 580 = 33$ K
m = 11052.09 g
If one pellet has 14 g of PCM material, then 789 pellets would be required to produce $1kWh_{th}$ energy. A 1600 MWh_{th} storage system to provide about 75% capacity factor to 100MW plant would require about 1.26 B capsules of this PCM.
Total Cost of TES system has been estimated to be as little as $14 and as high as $19 depending upon the composition of PCM and encapsulation materials.

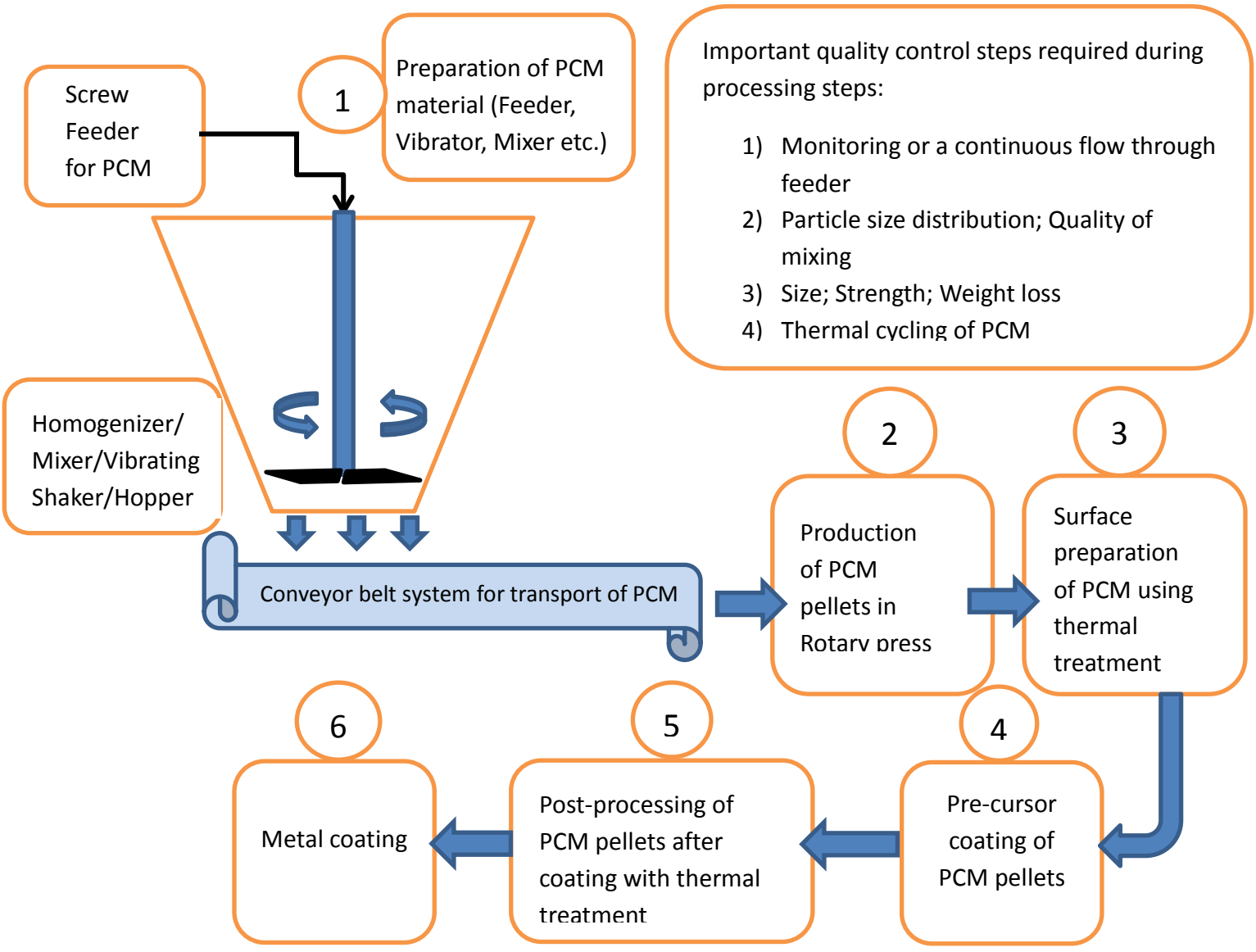
Screw Feeder for PCM
1
Preparation of PCM material (Feeder, Vibrator, Mixer etc.)
Important quality control steps required during processing steps:
1) Monitoring or a continuous flow through feeder
2) Particle size distribution; Quality of mixing
3) Size; Strength; Weight loss
4) Thermal cycling of PCM
Homogenizer/ Mixer/Vibrating Shaker/Hopper
Conveyor belt system for transport of PCM
2
Production of PCM pellets in Rotary press
3
Surface preparation of PCM using thermal treatment
4
Pre-cursor coating of PCM pellets
5
Post-processing of PCM pellets after coating with thermal treatment
6
Metal coating

CONCLUSIONS

- We have successfully developed encapsulated PCM with provision for expansion/contraction during melting/freezing
- Characterized the PCMs of interest
- Tested capsules for thermal cycling
  - Exceeded the 1st Phase milestone of 50 cycles
  - Successfully completed 200 cycles (continuing)
- Developed a numerical model for melting/solidification
- Developed a manufacturing plan for capsules
- Cost estimate of a TES system based on the developed PCM capsules – \$14/kWh$_{th}$ (<< than goal of \$20)
- Successfully met all the 1st Phase goals
- Preliminary discussions with companies on further testing and development for commercialization